Polarization-resolved cross-correlated (C2) imaging of a photonic bandgap fiber

Research Article | Vol. 24, No. 24 | 28 Nov 2016 | OPTICS EXPRESS 27785

Optics EXPRESS

Polarization-resolved cross-correlated (C^2) imaging of a photonic bandgap fiber

JOEL CARPENTER,[1,2,*] BENJAMIN J. EGGLETON,[2] AND JOCHEN SCHRÖDER[2,3]

[1]*School of Information Technology and Electrical Engineering, The University of Queensland, Brisbane, Queensland 4072, Australia*
[2]*Centre for Ultrahigh bandwidth Devices for Optical Systems (CUDOS), Institute of Photonics and Optical Science (IPOS), School of Physics, University of Sydney, NSW 2006, Australia*
[3]*Photonics Laboratory, Department of Microtechnology and Nanoscience, Chalmers University of Technology, SE-412 96, Göteborg, Sweden*
**j.carpenter@uq.edu.au*

Abstract: We demonstrate polarization-resolved frequency domain cross-correlated (C^2) imaging to characterize a 5m length of hollow-core photonic bandgap fiber. We produce a spectrogram of the fiber response to investigate the spatial, polarization, spectral, and temporal behavior. We then show how this temporally-resolved technique can be used to characterize multiple fiber launch conditions simultaneously by assigning each a unique time delay.

OCIS codes: (060.2270) Fiber characterization; (060.4005) Microstructured fibers.

References and links

1. O. Shapira, A. F. Abouraddy, J. D. Joannopoulos, and Y. Fink, "Complete modal decomposition for optical waveguides," Phys. Rev. Lett. **94**(14), 143902 (2005).
2. T. Kaiser, D. Flamm, S. Schröter, and M. Duparré, "Complete modal decomposition for optical fibers using CGH-based correlation filters," Opt. Express **17**(11), 9347–9356 (2009).
3. D. Flamm, O. A. Schmidt, C. Schulze, J. Borchardt, T. Kaiser, S. Schröter, and M. Duparré, "Measuring the spatial polarization distribution of multimode beams emerging from passive step-index large-mode-area fibers," Opt. Lett. **35**(20), 3429–3431 (2010).
4. J. Carpenter, B. J. Eggleton, and J. Schröder, "110x110 Optical Mode Transfer Matrix inVersion," Opt. Express **22**(1), 96–101 (2014).
5. N. K. Fontaine, R. Ryf, M. A. Mestre, B. Guan, X. Palou, S. Randel, Y. Sun, L. Gruner-Nielsen, R. V. Jensen, and R. Lingle, "Characterization of Space-Division Multiplexing Systems using a Swept-Wavelength Interferometer," in *Optical Fiber Communication Conference/National Fiber Optic Engineers Conference 2013*, OSA Technical Digest (Online) (Optical Society of America, 2013), p. OW1K.2.
6. J. Carpenter, B. J. Eggleton, and J. Schröder, "Reconfigurable spatially-diverse optical vector network analyzer," Opt. Express **22**(3), 2706–2713 (2014).
7. J. Carpenter, B. J. Eggleton, and J. Schröder, "Observation of Eisenbud–Wigner–Smith states as principal modes in multimode fibre," Nat. Photonics **9**(11), 751–757 (2015).
8. J. W. Nicholson, A. D. Yablon, S. Ramachandran, and S. Ghalmi, "Spatially and spectrally resolved imaging of modal content in large-mode-area fibers," Opt. Express **16**(10), 7233–7243 (2008).
9. D. N. Schimpf, R. A. Barankov, and S. Ramachandran, "Cross-correlated (C2) imaging of fiber and waveguide modes," Opt. Express **19**(14), 13008–13019 (2011).
10. D. N. Schimpf and S. Ramachandran, "Polarization-resolved imaging of an ensemble of waveguide modes," Opt. Lett. **37**(15), 3069–3071 (2012).
11. T. Cižmár, K. Dholakia, T. Čižmár, and K. Dholakia, "Exploiting multimode waveguides for pure fibre-based imaging," Nat. Commun. **3**, 1027 (2012).
12. J. Carpenter, B. J. Eggleton, and J. Schröder, "First demonstration of principal modes in a multimode fibre," in *European Conference on Optical Communication, ECOC* (Institute of Electrical and Electronics Engineers Inc., 2014).
13. J. W. Nicholson, L. Meng, J. M. Fini, R. S. Windeler, A. DeSantolo, E. Monberg, F. DiMarcello, Y. Dulashko, M. Hassan, and R. Ortiz, "Measuring higher-order modes in a low-loss, hollow-core, photonic-bandgap fiber," Opt. Express **20**(18), 20494–20505 (2012).
14. J. W. Nicholson, A. D. Yablon, J. M. Fini, and M. D. Mermelstein, "Measuring the Modal Content of Large-Mode-Area Fibers," IEEE J. Sel. Top. Quantum Electron. **15**(1), 61–70 (2009).
15. D. R. Gray, S. R. Sandoghchi, N. V. Wheeler, N. K. Baddela, G. T. Jasion, M. N. Petrovich, F. Poletti, and D. J. Richardson, "Accurate calibration of S(2) and interferometry based multimode fiber characterization techniques," Opt. Express **23**(8), 10540–10552 (2015).

#268921 http://dx.doi.org/10.1364/OE.24.027785
Journal © 2016 Received 16 Sep 2016; revised 11 Nov 2016; accepted 14 Nov 2016; published 21 Nov 2016

Optics EXPRESS

16. B. Sevigny, G. Le Cocq, C. C. C. Carrero, C. Valentin, P. Sillard, G. Bouwmans, L. Bigot, and Y. Quiquempois, "Advanced S^2 Imaging: Application of Multivariate Statistical Analysis to Spatially and Spectrally Resolved Datasets," J. Lightwave Technol. **32**, 4606–4612 (2014).
17. J. Demas and S. Ramachandran, "Sub-second mode measurement of fibers using C2 imaging," Opt. Express **22**(19), 23043–23056 (2014).
18. F. Poletti, N. V. Wheeler, M. N. Petrovich, N. Baddela, E. N. Fokoua, J. R. Hayes, D. R. Gray, and D. J. Richardson, "Towards high-capacity fibre-optic communications at the speed of light in vacuum," Nat. Photonics **7**(4), 279–284 (2013).
19. J. M. Fini, J. W. Nicholson, B. Mangan, L. Meng, R. S. Windeler, E. M. Monberg, A. DeSantolo, F. V. DiMarcello, and K. Mukasa, "Polarization maintaining single-mode low-loss hollow-core fibres," Nat. Commun. **5**, 5085 (2014).
20. A. F. Fercher, K. Mengedoht, and W. Werner, "Eye-length measurement by interferometry with partially coherent light," Opt. Lett. **13**(3), 186–188 (1988).
21. D. Lorenser, X. Yang, R. W. Kirk, B. C. Quirk, R. A. McLaughlin, and D. D. Sampson, "Ultrathin side-viewing needle probe for optical coherence tomography," Opt. Lett. **36**(19), 3894–3896 (2011).
22. J. Jasapara and A. D. Yablon, "Spectrogram approach to S2 fiber mode analysis to distinguish between dispersion and distributed scattering," Opt. Lett. **37**(18), 3906–3908 (2012).
23. R. G. H. van Uden, C. M. Okonkwo, H. Chen, H. de Waardt, and A. M. J. Koonen, "Time domain multiplexed spatial division multiplexing receiver," Opt. Express **22**(10), 12668–12677 (2014).
24. S. G. Leon-Saval, A. Argyros, and J. Bland-Hawthorn, "Photonic lanterns," Nanophotonics **2**(5-6), 429 (2013).

1. Introduction

Many techniques exist for the characterization of multimode optical waveguides [1–12]. Spatially and spectrally (S^2) resolved imaging [8,13,14] has become a popular technique for characterizing the modal content of optical fibers, due to its experimental simplicity and the fact that it requires no a priori knowledge regarding the fiber being characterized. However S^2 imaging does have limitations which arise from the fact that it only measures the amplitude of the spectral information, neglecting phase. Hence, it requires the presence of a dominant mode, ideally the fundamental mode, which acts as a reference against which the other far weaker modes interfere. Interference amongst the weaker modes is neglected. S^2 imaging also cannot differentiate between positive and negative time delay. These deficiencies have given rise to many techniques which either attempt to improve the accuracy of S^2 imaging through more advanced data processing [15,16] or through more advanced experimental techniques such as cross-correlated (C^2) imaging [9,10,17] which overcomes the limitations of S^2 imaging through the use of an external reference arm.

C^2 was implemented first in the time-domain [9] and then later in the frequency-domain [17] which can have advantages such as faster acquisition time and higher dynamic range. Previously, a frequency-domain C^2 system was implemented which analysed a single polarization at the output of the fibre [17]. The modes which propagate in optical fibres, particularly in the presence of mode coupling, are in general not linearly polarized. Rather they are vector modes with spatially-dependent polarization states. Hence in order to fully characterize a fiber's output beam, it is necessary to also include polarization information. Polarization-resolved C^2 imaging has previously been demonstrated in the time-domain [10].

In this paper we extend frequency-domain C^2 to include full polarization-resolved measurements. We demonstrate this technique to characterize the modal properties of a hollow core photonic band-gap fibre (HC-PBGF) [13,15,18,19]. This air-guidance mechanism of this fiber type is attractive for its low nonlinearity, low latency and potentially low loss [18]. The large design parameter space of the fiber also allows the modal and spectral properties of the fiber to be tailored in a way which is impossible for traditional solid core fibers and in combination with its difficult manufacture process makes it a good test case for new fiber characterization techniques [13,15].

2. Experimental setup

The experimental setup is illustrated in Fig. 1(a). The principle of C^2 imaging is similar to that of Optical Coherence Tomography [20,21] (OCT) in biomedical imaging. Both techniques measure a sequence of images corresponding with different delays as illustrated conceptually in Fig. 1(b). For OCT, this represents different depths into the sample being measured and for C^2 these represent different propagation delays which in turn correspond with different modes

Optics EXPRESS

of the fiber-under-test. The system of Fig. 1(a) consists of a Luna Technologies OVA-5000 swept-wavelength interferometer (SWI) which is attached to SLM systems at either end of the hollow-core photonic bandgap fiber. The SWI measures 32768 wavelength points in the C-band (1525-1566.7nm) and performs the initial data processing internally, outputting wavelength-dependent Jones matrices.

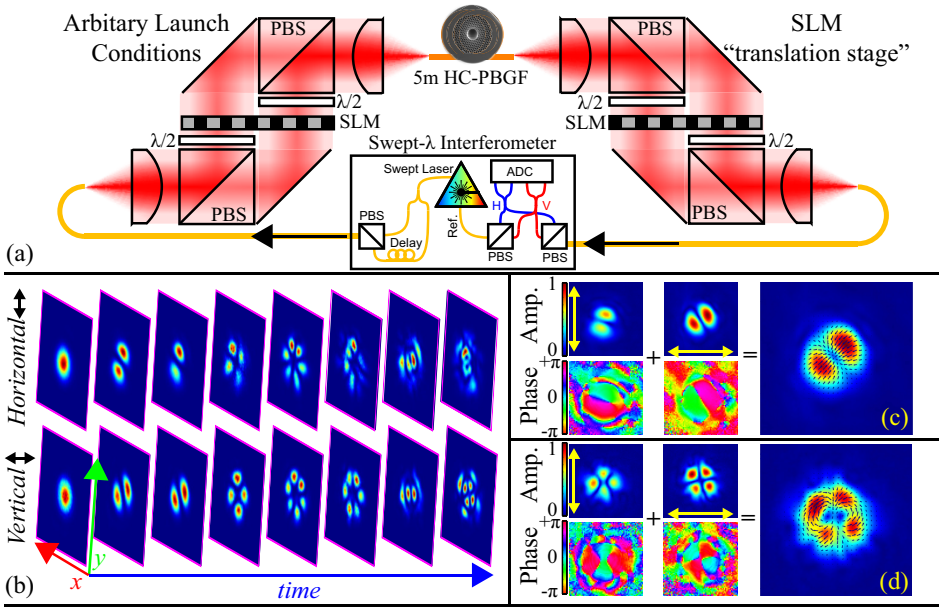

Fig. 1. (a) Experimental setup. (b) Illustration of C^2 imaging data set, consisting of x vs. y vs. time datacube for both output polarizations. (c-d) Examples of the spatially-dependent polarization states of two different delay times, corresponding to $LP_{1,1}$ and $LP_{2,1}$-like modes.

The SLM at the input of the fiber can be used to generate arbitrary launch conditions for characterization, while the SLM at the output in this case is simply performing the function of an x-y translation stage in traditional S^2 imaging [14] by rastering a 4.16μm mode-field diameter (MFD) Gaussian sampling spot across the output facet of the fiber-under-test. As for S^2 imaging, an alternative to rastering would be the use of a polarization-diverse imaging system with a camera. The specifics of which approach is faster will depend on the camera's frame rate, laser sweep rate and the SLM frame rate or mechanical update rate of the raster stage. For the most common use cases, a camera based approach would be quicker as it allows more spatial information to be acquired in parallel. A raster scanning approach can be faster if the measurement requires many wavelength points but few modes. Raster scanning can offer superior dynamic range and noise as a single mode detector will typically have better performance than a camera. Cameras may also be prohibitively expensive or difficult to obtain for certain wavelengths. The principles of the system shown in Fig. 1(a) can be applied to other fiber types and wavelength bands, with the most appropriate choice for implementing each aspect dependent on the measurement requirements and equipment availability.

For each spatial sampling position (x,y) a wavelength sweep is performed with the SWI yielding the wavelength/frequency dependent Jones matrices between the fiber input and the sampling point at the output. In this way, in addition to both polarizations being analyzed at the output of the fiber, two launch conditions corresponding to both orthogonal polarizations at the input are also measured in the same sweep. Hence, with the SLM at the input, it is possible to configure the launch conditions to an arbitrary spatially dependent polarization state. Given that the system measures the amplitude and phase of both output polarizations as illustrated in Fig. 1(b), it is possible to construct the full spatially-dependent polarization states of the modes as shown in Fig. 1(c) and Fig. 1(d), which show examples for $LP_{1,1}$ and

Optics EXPRESS

$LP_{2,1}$-like modes respectively. The time evolution of the electric field for these examples is animated in Visualization 1 and Visualization 2.

3. Experimental results

3.1 Spatial and polarization resolved impulse response

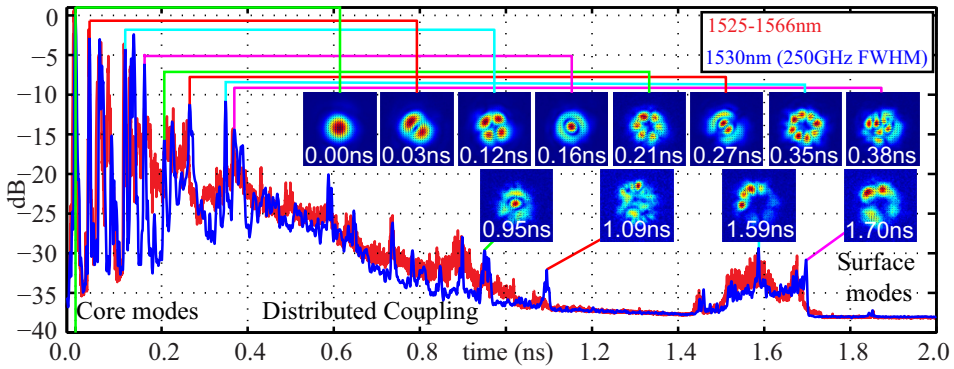

Fig. 2. Fiber impulse response including spatially and polarization resolved images for selected delays at 1530nm.

In this demonstration, the fiber-under-test is a 5m length of NKT Photonics 19-cell HC19-1550 hollow-core photonic bandgap fiber. The fiber was coiled and taped to the optical table on an approximately 20cm diameter. The SLM is configured to launch a superposition of lower-order modes, $LP_{0,1}$, $LP_{1,1}$, $LP_{0,2}$ and $LP_{2,1}$ with approximately equal weighting and the resulting impulse response at each spatial position at the output measured using the SLM and SWI. The impulse response of the fiber launch is shown in Fig. 2 both for the total optical bandwidth measured (1525-1566.7nm) as well as an example of the impulse response with a Gaussian filter applied at 1530nm with a 250GHz FWHM bandwidth. The measured impulse response contains both mode dispersion and chromatic dispersion and as is indeed the case for this fiber, it is possible for two different spatial modes to have the same group-delay at two different wavelengths. Hence where chromatic dispersion is significant, it is appropriate to analyse the impulse response filtered to relatively narrow bandwidths so as the individual spatial modes can be observed with the chromatic effects removed [13,22]. The spatial profiles illustrated in Fig. 2 are taken from the impulse response at 1530nm. The impulse response is qualitatively similar to previously observed impulse responses in photonic bandgap fibre [13]. There are several discrete peaks corresponding to air modes (also known as core modes) with spatial profiles similar to the lower-order $LP_{l,m}$ type modes of a solid-core fiber. In this fiber as shown in Fig. 2, $LP_{0,1}$, $LP_{1,1}$, $LP_{2,1}$, $LP_{0,2}$, $LP_{3,1}$, $LP_{1,2}$, $LP_{4,1}$ and $LP_{2,2}$-like discrete modes can be observed up to 0.38ns. The discrete peaks are followed by a continuum of delays corresponding with strong distributed mode coupling. Finally, at the largest delays, light arrives which has travelled mostly as surface modes along the length of propagation. Surface modes are primarily confined to the silica ring and struts around the fiber's centre hole as can be seen in the two largest delay (1.59 and 1.70ns) images of Fig. 2.

3.2 Spectrogram analysis

By performing a sliding window Fourier transform [5,13,22] we obtain the spectrogram of Fig. 3. containing the spectrally filtered (250GHz FWHM) responses for many wavelength bands. With this a more detailed description of the spatial and spectral behavior of the fibre is obtained which can differentiate between modal and chromatic effects. Across the entire band, the trend is the same; multiple discrete peaks at short delays, increasingly turning into a continuum of delays corresponding with modes undergoing distributed coupling of decreasing strength beyond approximately 0.4ns of delay, before a final diffuse set of peaks at delays beyond 1.4ns for the surface modes. The modal dynamics are far more complicated than

Optics EXPRESS

traditional solid-core fibers. A comprehensive 'fly-through' of the spectrogram of Fig. 3 is provided in Visualization 3, which illustrates the spatial and polarization properties for each time delay step in 5nm wavelength spacings from 1530 to 1565nm.

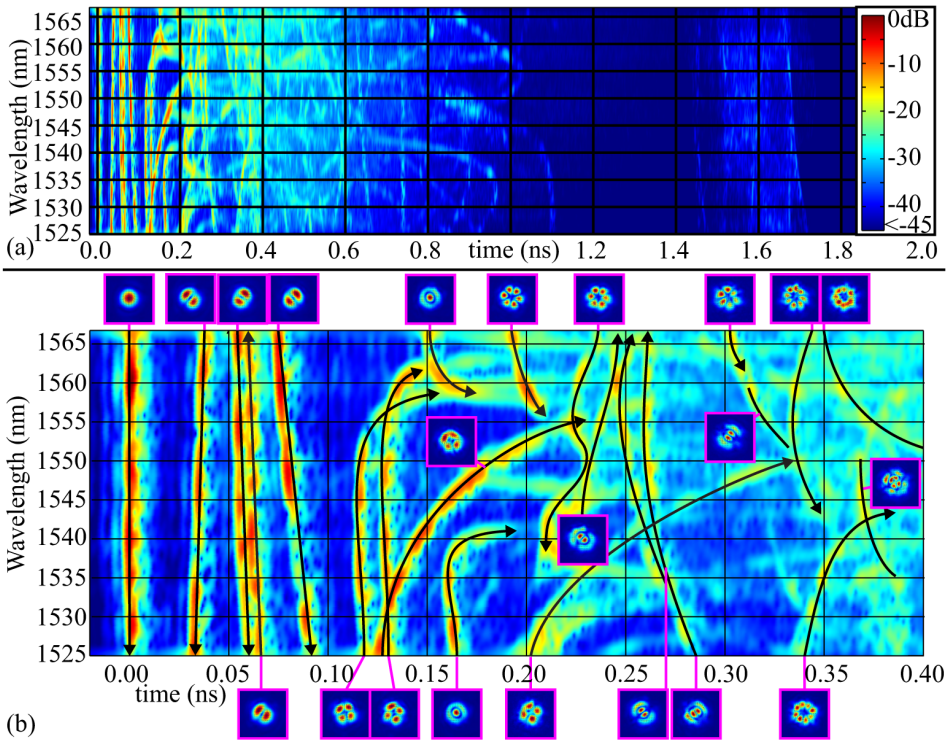

Fig. 3. Spectrogram of fiber response. (a) Full impulse response (b) First 0.4ns of impulse response with selected lower-order modes indicated.

Figure 3(b) contains the first 0.4ns of the spectrogram of Fig. 3(a), where individual modes can still be easily identified before the continuum of mode scattering for larger delays. As has been previously observed [13], the $LP_{1,1}$-like mode family is split into four non-degenerate modes. Similarly, splitting between the $LP_{2,1}$ modes is also observed, with the splitting being significantly larger than for the $LP_{1,1}$ modes. It can also be observed that two of the $LP_{2,1}$ modes cross at approximately 1530nm. The most dispersive of the $LP_{2,1}$ modes, which starts with a delay of approximately 0.2ns at 1525nm is a good example of how the spectrogram approach is useful for differentiating between the spatial and spectral properties of the modes. This mode intersects multiple other modes at multiple wavelengths and as a result it is not possible to observe this $LP_{2,1}$ mode in isolation at most wavelengths. However from observation of the spectrogram it is possible to find certain wavelength bands, in this case between 1545 and 1550nm, in which the mode happens to exist relatively clear of other modes so as their individual structure can be observed. The $LP_{2,2}$ (0.37ns,1545nm) is another example.

As the modes become of increasingly high order their properties become increasingly complicated. Two orthogonally polarized $LP_{0,2}$ modes are observed, both with delays of approximately 0.16ns, but do not appear to propagate at the same wavelength. One being cutoff above 1542nm and the other not propagating below 1558nm. The $LP_{1,2}$ modes appear to be split into four non-degenerate types, with very different dispersion. Two appear to split from one another at approximately 1535nm and 0.27ns of delay. Another variant begins to propagate at 1540, with a shorter delay of 0.23ns and the fourth type appears to largely be lost amongst other modes and distributed coupling except for a band between 1550 and 1560nm where it can be seen propagating at a delay of approximately 0.32ns. $LP_{3,1}$ and $LP_{4,1}$ modes

Optics EXPRESS

are also observed with large splittings and varied chromatic dispersion although the complete set of four modes for each type are not so easily identifiable. Some individual modes can also be observed beyond 0.4ns including those with similar profiles to the traditional solid-core LP modes, as well as photonic bandgap specific mode types. A comprehensive examination of these can be obtained by observation of Visualization 3.

3.3 Time-multiplexed C^2 imaging

Just as for other fully time-resolved characterization techniques [5–7,23] it is possible to measure multiple launch conditions in the same measurement by assigning each launch a unique delay. The number of possible launches which can be measured simultaneously will depend on the dynamic range of the measurement as the total power is split amongst multiple launches, but primarily on the number of impulse responses which can fit within the maximum delay measurable by the SWI. This depends on the wavelength resolution of the sweep and for the Luna Technologies OVA-5000 used here, the maximum delay is 6.26ns. These multiple launch conditions could be different phase masks for exciting specific modes [5], a photonic lantern [24] or as in this case, multiple offset spots [11]. In this way, it would be possible to characterize the entire mode basis of the fibre in a single measurement.

Figure 4 presents the impulse response of the fibre where two spot launches have been measured simultaneously. Power from the SWI is split in half and sent into a fibre array which is imaged onto the core of the fiber-under-test such that there are two Gaussian spots of 4.16μm MFD spaced by 20μm with one spot aimed at the centre of the fiber core. The offset spot is delayed by 2.6ns as shown in Fig. 4 with green lines indicating the delay of the fundamental mode for both launch conditions. As the SWI itself also uses time multiplexing to measure both orthogonal polarizations in a single sweep, there are in fact 4 launch conditions being measured simultaneously corresponding with both polarizations for both offset launches. Visualization 4 animates each of the 4 launch conditions as a function of delay in detail. Both the launch at the centre and at an offset have the same basic features and observable modes as the previous example, with discrete peaks at low delays followed by a continuum of scattered modes. Albeit it with different relative mode strengths.

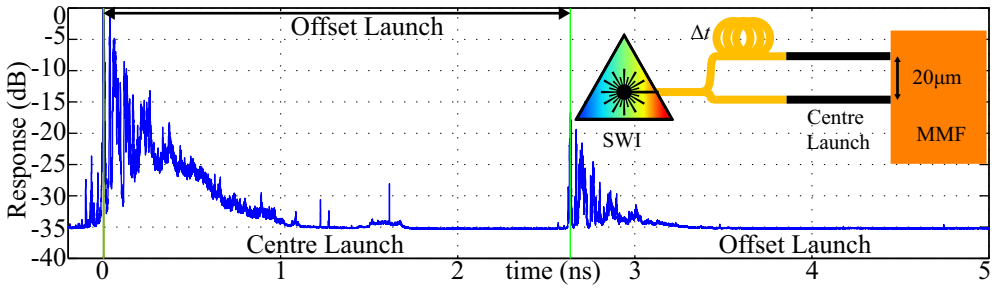

Fig. 4. Time-multiplexed C^2 imaging response. Two independent fiber launch conditions being obtained in the same measurement by assigning each launch a different delay. Time-axis defined relative to centre launch $LP_{0,1}$ mode.

4. Conclusion

We have demonstrated polarization-resolved frequency domain cross-correlated (C^2) imaging of a hollow-core photonic bandgap fiber. We applied sliding-window Fourier transform (spectrogram) analysis to differentiate between the spatial and spectral mode dynamics in the fiber. Finally, we demonstrated how the temporally-resolved nature of this technique can be used to characterize multiple launch conditions in the same measurement.

Funding

Australian Research Council: Linkage (LP120100661); Laureate Fellowship (FL120100029); Centre of Excellence (CUDOS, CE110001018); and DECRA (DE120101329).